DOI: 10.13009/EUCASS2017-395

Evaluation of the Grid Convergence for a Rocket Combustion Chamber with a Porous Injector

Victor P. Zhukov⋆ and Klaus P. Heinrich
Institute of Space Propulsion, German Aerospace Center (DLR)
Langer Grund, 74239 Hardthausen, Germany
victor.zhukov@dlr.de · klaus.heinrich@dlr.de
⋆Corresponding author

Abstract

The purpose of the present study is to quantify the grid convergence in simulations of rocket combustion chambers performed with the averaged Navier–Stokes equations. The present work is a continuation of the previous studies on simulations of rocket combustion chambers with porous injector head API-68. Turbulence is modelled by the SST turbulence model; turbulent combustion is modelled using the extended eddy-dissipation model developed earlier. The grid convergence study is carried out for two injector configurations on five meshes for each configuration. Results shows that the dependences of the flame length and wall heat flux on mesh spacing is described well by a parabola, and the modelling using the current model requires a spacing of around 30 μm.

1. Introduction

A situation on the space launch market, pricing pressure from private spaceflight companies, and a desire to reduce cost from government space agencies establish new requirements for rocket engines. Now rocket engines should be cost-effective. It does not mean that rocket engines should be cheap because it may increase other costs, but they should be cost-effective within the complex for cargo delivery to orbit. One of the developments aimed at cost reduction is an Advanced Porous Injector (API). This is a concept of injector head for rocket engines, which is under development at the German Aerospace Center (DLR-Lampoldshausen) in the last decade. [1] Advanced porous injector allows reducing cost while achieving better performance. In API injector, fuel is fed into combustion chamber through a porous plate; oxidizer is fed through many small injectors uniformly distributed over the injector plate similar to showerhead. [1]

Thermal management is a key problem of rocket engine design. In recent work, Zhukov and Suslov studied wall heat fluxes in a combustion chamber with injector API-68 carrying out hot-run tests and fluid simulations. [2] Computational Fluid Dynamics (CFD) simulations are also a way to reduce cost during development phase. The comparison of the results of work[2] with the results of the previous attempt to simulate the flow in the combustion chamber with API-68[3] shows that there is an impact of numerical grid spacing on the simulation results. The numerical mesh increased from 2.6 Mio cells in the first simulations[3] to 6.2 Mio cells in the final simulations.[2] At the same time, the flame grew in the length from 3 cm to 5 cm. However, during the work on obtaining the final results it was found that the further increase of the mesh size does not lead to a significant changes in the simulating results. [2] Nevertheless, the problem of the quantitative characterization of mesh effect was not solved in the work, [2] and it is still actual. The aim of the present work is the quantification of the grid convergence and the evaluation of the numerical error associated with spatial discretization.

First, it is necessary to say few words about the object of the research. The main part of porous injector API-68 is a porous plate sintered from bronze beads with a diameter around 0.6 mm. The plate is permeated by 68 stainless steel tubes of small diameter, which are practically uniformly distributed over the porous plate. These tubes are oxygen injectors. They have a plain geometry and a sharp cut (no tapering nor recess). The oxygen injectors have an outer diameter of 2 mm and an inner diameter of 1.5 mm (this value was incorrectly given in Table 3 of previous article [2]). Hydrogen is fed uniformly through the porous plate. The photograph of API-68 can be found in works. [1–4] API-68 demonstrated a high combustion efficiency in a wide range of parameters. [1]

The combustion chamber used in works[2,3] is a copper cylindrical chamber with a diameter of 50 mm and consists of separate segments. The segments allows measuring wall temperature, wall heat flux and static pressure along the chamber axis with a spatial resolution of 50 mm.

DOI: 10.13009/EUCASS2017-395

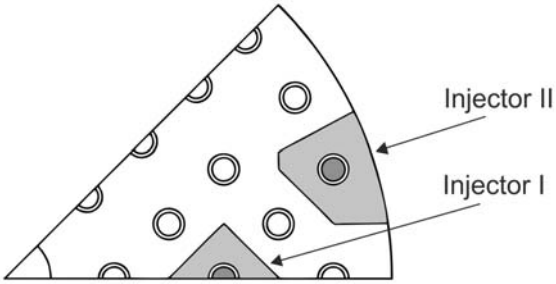

Figure 1: Arrangement of injectors in the porous injector head

2. Modelling

The flow in the studied combustion chamber is very nonuniform. Grid resolution plays a role only in areas of high gradients. Therefore, there is no need to perform a grid convergence study in the whole domain. The region, where the mesh effect was observed, is only the vicinity of flame. Here are the highest gradients of pressure, densities and velocities. Because the limit of the computational power of currently used workstations was reached in previous work, [2] the present grid convergence study has been performed on single injectors of the porous injector head. For the grid convergence study, two injectors have been chosen: one in the middle of the injector plate and one near the sidewall, see Fig. 1. The arrangement of separate oxygen injectors has rectangular pattern in API-68 and can be represented by a sector of 45°. For this reason, only eighth part of the combustion chamber was modelled to save a computational time in work.[2] Here, in order to reduce computational cost, the numerical domain is further reduced to single injectors. The injectors chosen for the present study are shown in Fig. 1 as Injector I and Injector II. Injector I was chosen because it can be represented in a very simple domain. All of its sidewalls are symmetry planes. Injector II stays closer to the sidewall than other injectors, so it has the largest impact on wall heat flux. The numerical domains of Injectors I and II have also part of the oxygen injector. It is a plain cylindrical tube with a diameter of 1.5 mm and a length of 15 mm located upstream of the injector plate. The part of oxygen injector is needed to form a realistic exit velocity profile.

In the present study, the same physical model and numerical setup are used as in our previous work. [2] (For the detail description of the physical model and of the numerical setup please see original paper. [2]) Nevertheless, the main points of the numerical model, which directly affect the results of the present study, are given below. The flow is modelled using the Favre-averaged Navier–Stokes equations. The simulations have been performed using the commercial CFD code ANSYS CFX.[5] All governing equations excluding the equations for enthalpy and for mass fractions of mixture components have been solved using "High Resolution" advection scheme. [5] This scheme reduces to the first order near discontinuities and is as close as possible to the second order as possible without violating boundedness principle.[6] The transport equations for enthalpy and for the mass fractions of mixture components have been solved using the first order upwind differencing scheme. The first order scheme has been used because of divergence in the solver during use of the high resolution scheme. The reason of the divergence is numerical dispersion due to high gradients of temperature and mass fractions.

Turbulence has been modelled using the SST $k-\omega$ turbulence model. [5] Turbulent combustion has been modelled using the extended eddy-dissipation model. In this model, the degree of the chemical reaction is regulated by a special parameter called "Maximum flame temperature". This parameter in fact sets the temperature of burnt gases in correspondence with the local mass ratio of oxygen atoms to hydrogen atoms in the mixture. (This ratio oxygen-to-hydrogen plays a role similar to equivalence ratio.) Flame temperatures are calculated using the program NASA Chemical Equilibrium with Applications (CEA).[7] One can find other details of the numerical model in our recent works.[2,8,9]

Finally, it is necessary to give a brief description of applied boundary conditions. Oxygen is fed through the tube in the middle of the domains; hydrogen is fed through the surface of the injector plate. They are separated by a small ring (injector tip), which has a thickness of 0.25 mm. Figure 2 gives an overall picture of the arrangement of boundary conditions. Propellants are injected at cryogenic temperatures and with velocities, which are calculated in the assumption that propellants are uniformly distributed over the cross-section of the injector head. The values of temperatures and mass flow rates as well as other boundary conditions have been taken from work [2] and are presented in Table 1. At the outlet, pressure has been set; in the case of Injector I, all sidewalls are symmetry planes.

DOI: 10.13009/EUCASS2017-395

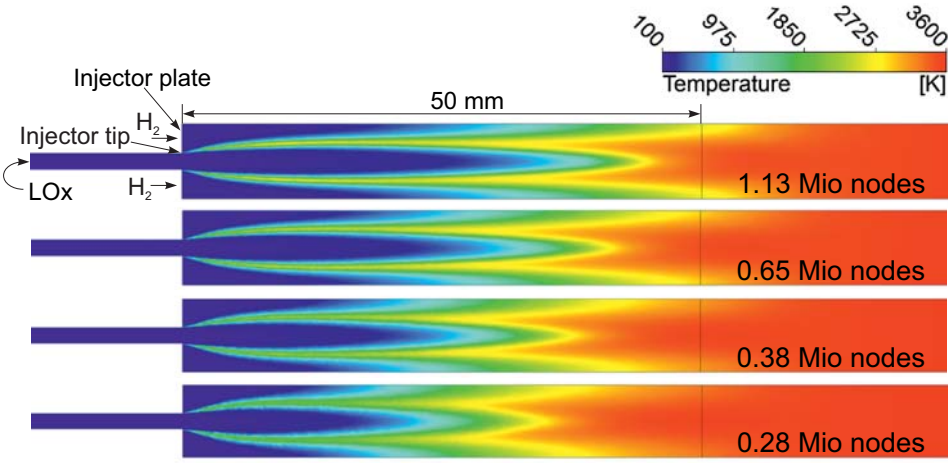

Figure 2: Flame of Injector I at four different mesh densities

Table 1: Boundary conditions for the simulation according to Zhukov and Suslov [2]

Injection velocity, O_2	13.56 m/s
Temperature, O_2	120 K
Injection velocity, H_2	9.10 m/s
Temperature, H_2	100 K
Mass ratio of oxidizer-to-fuel (ROF)	6[a]
Pressure at the outlet	~75.5 bar

[a] Average value for the combustion chamber

3. Grid convergence study

The effect of mesh was already observed in earlier work.[2] The effect manifested itself in an elongation of the flame. The flame had a spindle shape and became slightly longer with the mesh refinement without changing its shape and other characteristics. The aim of the present work is to quantify the grid convergence for the case of a combustion chamber with the porous injector used in work.[2] The grid convergence study was carried out using five grids for both Injector I and II. The mesh from previous work[2] was taken as a baseline mesh. This unstructured mesh consists of tetrahedral elements with prism layers on walls. The mesh is nonuniform and is refined in a flame region, near sidewalls, and around oxygen posts (walls which separate oxygen from hydrogen). The spacing (a distance between nodes) at the tip of oxygen post amounts to about 18 μm. In the flame region, the spacing in average equals to 150 μm. The thickness of the first layer at the sidewalls grows in the axial from 4 μm to 8 μm. The mesh refinement in the flame region had a shape of cylinder with a diameter of about 6.5 mm and with a length of about 53 mm.

The grid convergence study has been performed on five numerical meshes for both Injector I and Injector II. Two of the five meshes have higher grid densities than the baseline mesh, and another two meshes have lower grid densities. The refinement factor in spacing equals to 1.26; the coarsing factor equals to 1/1.26, respectively. One of challenges, which are faced by researches during grid convergence studies, is that the number of nodes in numerical mesh grows very fast during mesh refinement in the three-dimensional (3D) case. The refinement factor of 2 means the increase of node number by eight times during mesh refinement. Often, simulations are carried out on meshes which are near to the limit of available computational resources. On the other hand, the coarsening of mesh is also often not possible because a coarse mesh may give physically incorrect results. In the present case, a refinement factor of 1.26 doubles the amount of nodes in one refinement step.

4. Results and discussion

4.1 Injector I

As it was already in the previous work, the flame length depends on mesh density (see Fig. 2). The parameters of gas in post-flame zone (temperatures, pressures, densities, mass fractions, etc.) do not show any sensitivity to the mesh

DOI: 10.13009/EUCASS2017-395

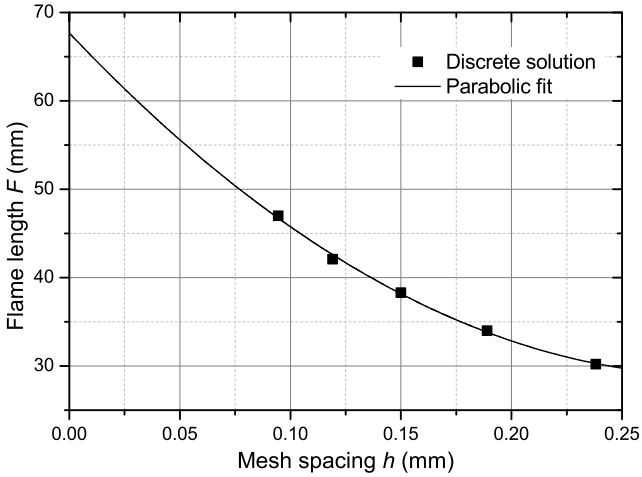

Figure 3: Flame length F as a function of mesh spacing h

density. In the present case, the flame length is a convenient parameter for the quantification of the grid convergence. First, the flame length has shown a higher sensitivity to the mesh density than other parameters of gas and flow. Secondly, it can be easily interpreted and measured. In our case, the flame length is defined as a distance from the injector plate to a point where temperature on the axis of the injector reaches 2000 K, which corresponds to the colour between green and yellow in Fig. 2. The flame front and boundary layers are the smallest objects in rocket combustion chambers. While the resolution of boundary layers is somehow a solvable problem, the resolution of flame front is a very hard task in case of rocket combustion chambers. The flame front is very thin at high pressures. The thickness of hydrogen–oxygen flames amounts to 100–200 μm at pressures of 50–100 bar. [10] Flame does not have a predetermined position in combustion chamber, so it is necessary to fill a relatively large volume of combustion chamber with a very fine mesh. When a mesh is too coarse for the flame front, errors occur in the evaluation of both mass fractions and their gradients at integration point. The use of coarse mesh alongside with low-order advection schemes increases the impact of numerical dissipation which results in the reduction of the flame length.

In Fig. 3, one can see the dependence of the flame length on spacing. The numerical model uses both first and second order advection schemes, and therefore the results are approximated by a mixed-order equation:

$$F(h) = F_{exact} + C_1 h + C_2 h^2 + O(h^3)\,, \tag{1}$$

where F is flame length, h is mesh spacing, and $F_{exact} := F(h \to 0)$. Neglecting third-order terms, we get

$$F(h) = F_{exact} + C_1 h + C_2 h^2. \tag{2}$$

The idea to use the mixed order equation came from the work by Roy who carried out the detailed analysis of grid convergence errors in the case of mixed-order numerical schemes. [11] As we can see in Fig. 3, the dependence of the flame length on spacing is described by parabola (Eq. (2)) very well.

Using Eq. (2) we can evaluate a spatial discretization error:

$$\frac{F_{exact} - F(h)}{F_{exact}} \times 100\%\,.$$

In Fig. 4 one can see the spatial errors in the flame length for different meshes. The graph also shows the first- and second-order error terms ($100\% \times C_1 h/F_{exact}$ and $100\% \times C_2 h^2/F_{exact}$) along with their sum.

First, one may notice that the spatial discretization error in the flame length for the tested meshes reaches relatively high values 30–60%. An acceptable value of the spatial error is reached at the mesh spacing of several tens of microns. The second order term rapidly declines with mesh spacing, and below 0.1 mm the spatial convergence has the first order. This result is not surprising because the transport equation for mass fractions, which plays a major role in this case, is discretized using the first-order advection scheme.

The difference in the magnitudes of the first- and second-order error terms at $h = 0.1$ mm emphasizes advantages of second-order schemes in comparison with first-order schemes. The first- and second-order error terms have different signs. At $h \approx 0.6$ mm, the flame length theoretically may reach the exact value of 67.7 mm; however, spatial discretization errors for other parameters (p, T, ρ, v_i, etc.) may be very large on such coarse mesh. Indeed, constants C_1 and C_2

DOI: 10.13009/EUCASS2017-395

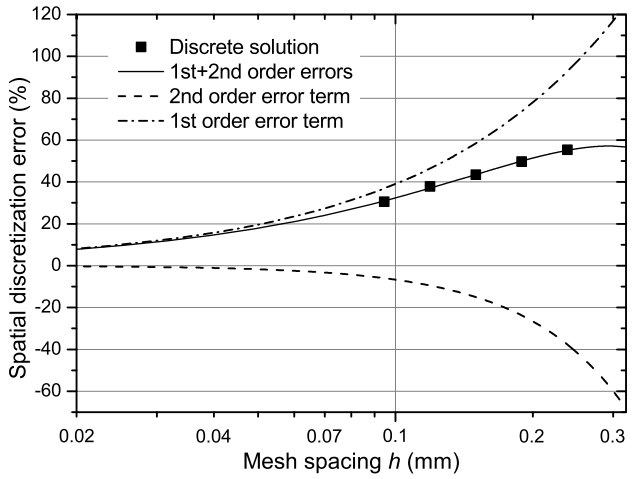

Figure 4: Spatial discretization error in the flame length as a function of mesh spacing h

in Eq. (1) have individual values for each parameter. While only the increase of the flame length has been observed during the mesh study, the numerical solution may be completely different on a much coarser mesh with spacing of 0.6 mm, so that spatial discretization errors for some parameters will reach 100%.

4.2 Injector II

Let us consider the case of Injector II. First, this case is more important than the previous case because the major goal of the CFD simulation of rocket combustion chambers is the predictions of heat transfer to walls. For the thermal loads of walls, the outer row of injectors is responsible where Injector II makes the largest contribution. The same numerical model as for Injector I has been used for Injector II in the simulations. The difference between the configurations is that one side of the numerical domain of Injector II has been treated as a no-slip isothermal wall. The sidewall has been divided into five segments of 50 mm length, where each segment has temperature in accordance with the measurements.[2] The roughness of walls has been set to 5 μm. The view of Injector II with temperature fields in the longitudinal section and on the sidewall is shown in Fig. 5. The simulation of Injector II is also characterized by the prolongation of the flame with mesh refinement in the same way as for Injector I. However, we consider the grid convergence for wall heat flux instead of flame length in this case because wall heat flux is the main goal of our CFD simulations.

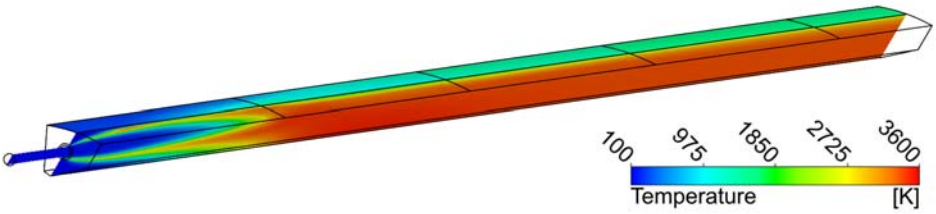

Figure 5: Simulation of Injector II, temperature fields in the longitudinal section and on the sidewall

The dependence of wall heat flux on spacing is shown in Figs. 6 and 7. (Here wall heat flux is an average value of heat flux on each segment, i.e. the average wall heat flux for each 50 mm in the longitudinal direction.) The dependence of wall heat flux on grid spacing is also described by parabola very well (i.e. by Eq. (2)). The influence of grid spacing (in absolute values) is maximum for Segment 2, which covers distances from the injector plate from 50 mm to 100 mm. Further, the impact of spacing decreases with the distance from the injector plate. It is worth noting that the graph in Fig. 7 has the significantly smaller chart scale on the vertical axis than the scale in Fig. 6. Using the same method as in the previous section, we calculated the spatial discretization error in the wall heat flux. The results of the calculations were compiled in one chart, see Fig. 8. The chart clearly shows that the impact of mesh decreases with the distance from injector plate and that the largest effect is observed for Segments 1 and 2. Such dependence of discretization error on axial distance is not surprising. For the tested meshes, the flame length varies from 30 to 50 mm. Hot gases reach the sidewall around 10 mm later, so the distance, at which hot gases touch the sidewall, varies from

DOI: 10.13009/EUCASS2017-395

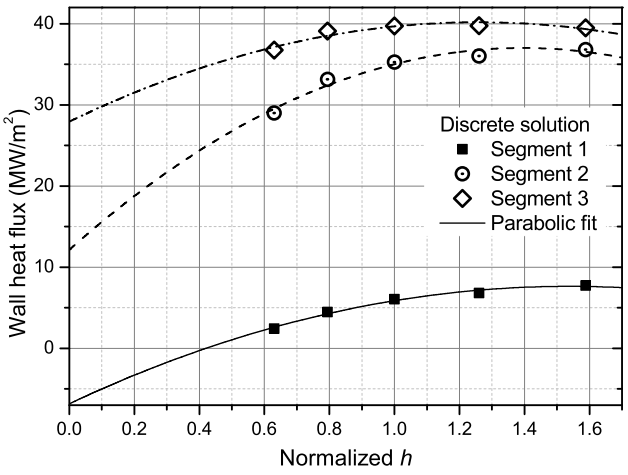

Figure 6: Wall heat flux in Segments 1, 2 and 3 as a function of mesh spacing h

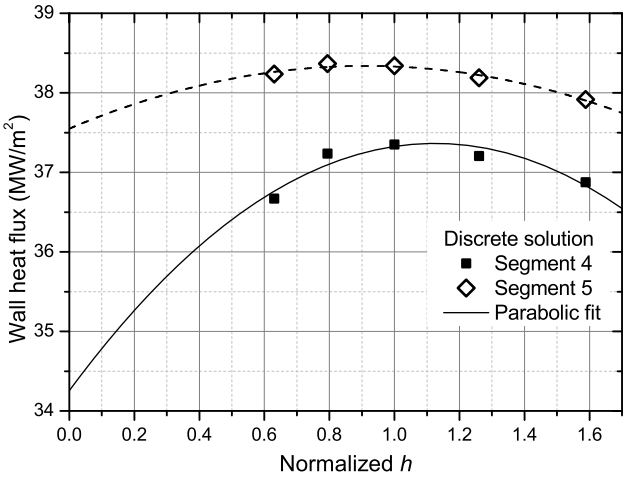

Figure 7: Wall heat flux in Segments 4 and 5 as a function of mesh spacing h

40 to 60 mm for different mesh spacing. Meanwhile, the border between Segments 1 and 2 is located at $x = 50$ mm, so the flame crosses the border of the segments. Behind the flame front, the temperature of hot gases is relative constant; therefore, the mesh impact on flow is low at large distances from the injector plate.

4.3 Discussion

Equation (2), which has been used to describe the mesh effect, has a mixed order. This has two important consequences. The first consequence is that the order of mesh convergence is defined by lower-order terms in the case of mixed order. The higher-order term becomes smaller than the lower-order term as spacing h tends to zero, which is shown in Fig. 4. The second consequence is that first- and second-order terms may have a different sign and compensate each other at a certain value of h. For a grid convergence study with a small number of meshes, this may look as a grid divergence or as an apparent independence of simulation from mesh density. Therefore, it is necessary to use at least four meshes in order to evaluate reliably the order of grid convergence, the level of spatial discretization error, and the current position on the parabola. (Eq. (2), which was used to describe the results, has three independent parameters.) If a grid convergence study is carried out with a small refinement factor, i.e. the mesh spacing is varied in a narrow range, and the spatial discretization error amounts to a few tens of percent, than it is necessary to use more than four meshes.

The transition from the mixed order to the second order is unlikely possible in simulations of rocket combustion chambers due to strong gradients of temperature, density, and species concentrations in flame. According to work, [10] the flame front thickness amounts to about 100 μm at the studied conditions while parameters of gas (temperature, density, etc.) change their value by orders of magnitude within the flame front. In the simulations the flame thickness is

DOI: 10.13009/EUCASS2017-395

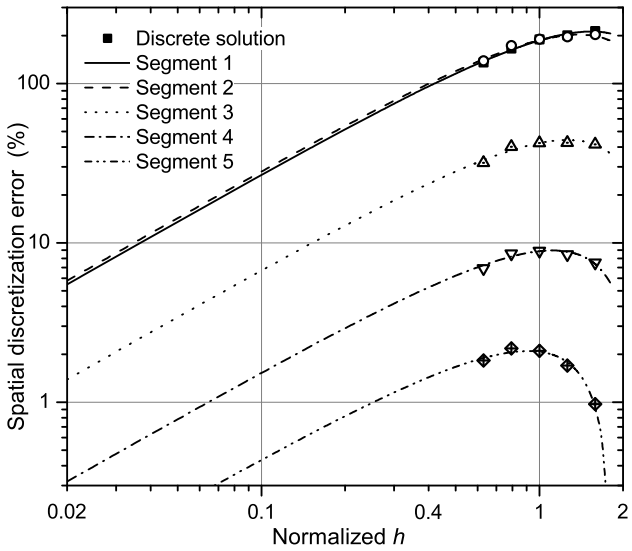

Figure 8: Spatial discretization error in the wall heat flux as a function of mesh spacing h

significantly larger due to model simplifications; however, it is still much less than 1 mm. The second-order advection schemes generate wiggles (or oscillations) near gradients what is called numerical dispersion. That is why, the first-order upwind scheme is used for the transport equations for H and Y_i (enthalpy and mass fractions), and for other variables (ρ, v_i, k, and ω) the "High Resolution" scheme is used which reduces from the second order to the first order near discontinuities. As a consequence, the obtained numerical solution is characterized by the mixed-order accuracy in mesh spacing.

With regard to the particular case considered here, the spatial discretization error of wall heat flux reaches very high values for Segments 1 and 2, see Fig. 8. In the case of Injector I (see Fig. 4), the model underpredicts the flame length with 10% error at $h = 30$ μm while this spacing still means the error of 50% in wall heat flux for Segments 1 and 2. (In Fig. 8, normalized h of 0.2 corresponds to $h = 30$ μm.) This large value of the error cannot be explained only by the increase of the flame length with mesh refinement and by passing the flame over the border of these segments. There is also a second reason for the large value of the spatial discretization error for wall heat flux. In contrast to the domain of Injector I, the domain of Injector II has the sidewall and a region where the flame touches the sidewall. The large value of the error is determined by relatively large cells in this region, where the flame interacts with the boundary layer. To get the solution with small discretization error for Injector II, it is necessary to have a mesh with another distribution of nodes (finer mesh) in the region where the flame touches the sidewall. As regards the simulations of the whole combustion chamber, the average spatial discretization error of wall heat flux is smaller because flames of other injectors do not penetrate into the boundary layer. Injector II was purposely selected among four outer injectors to estimate the maximum possible impact of mesh.

5. Conclusions

The grid convergence studies were carried for the flames of the two selected oxygen injectors: one in the middle of the injector head and one near the sidewall. The CFD simulations were performed by solving the averaged Navier–Stokes equations. The numerical solution was obtained using the first-order upwind scheme for the transport equations for H and Y_i and the "High Resolution" scheme for other variables: ρ, v_i, k, and ω. Therefore, the obtained solution is characterized by the mixed-order accuracy in space, when the solution depends on both h and h^2. To study the dependence on the mesh spacing h, the simulations were performed on five meshes for each injector. The meshes were generated using a global refinement/coarsening factor equal to $\sqrt[3]{2}$, so the number of nodes was increased twice after each refinement step. The grid convergence was studied for two parameters: flame length and wall heat flux, which are very important as a practical matter and have the largest sensitivity to mesh spacing.

The study showed that the accuracy of the simulation results is described by the mixed order in mesh spacing, namely by parabolic dependence on spacing h. Therefore, at least four different meshes are required for the accurate evaluation of the order and parameters of grid convergence. In the case of the small refinement factor, the reliable determination of convergence parameters requires more than four meshes. The first-order and second-order terms may

DOI: 10.13009/EUCASS2017-395

have a different sign which may lead to a false feeling that the grid convergence is reached already at a coarse mesh.

On simulations of the combustion chamber with porous injector API-68, the flame of single injectors can be simulated using the current model with spacing of around 30 μm. As for the wall heat flux predictions, they need a very fine mesh in the region where flame penetrates into the boundary layer.

References

[1] J. Deeken, D. Suslov, O. Haidn, S. Schlechtriem, Combustion efficiency of a porous injector during throttling of a LOx/H_2 combustion chamber, in: EUCASS Proceedings Series – Advances in AeroSpace Sciences, Vol. 2, 2011, pp. 251–264.

[2] V. P. Zhukov, D. I. Suslov, Measurements and modelling of wall heat fluxes in rocket combustion chamber with porous injector head, Aerosp. Sci. Technol. 48 (2016) 67–74.

[3] V. P. Zhukov, D. I. Suslov, O. J. Haidn, CFD simulation of flow in combustion chamber with porous injector head and transpirationally cooled walls, in: 4th European Conference for Aerospace Sciences, 2011, paper ID: 29.

[4] V. P. Zhukov, O. J. Haidn, Analytical study of stationary temperature field in transpiration cooled porous wall, P. I. Mech. Eng. G-J. Aer. 227 (5) (2013) 873–881.

[5] ANSYS, Inc., Canonsburg, PA, USA, ANSYS CFX-Solver Theory Guide, Release 14.5 (October 2012).

[6] T. J. Barth, D. C. Jespersen, The design and application of upwind schemes on unstructured meshes, in: 27th Aerospace Sciences Meeting, Aerospace Sciences Meetings, American Institute of Aeronautics and Astronautics, Reno, NV, U.S.A., 1989.

[7] B. J. McBride, S. Gordon, Computer program for calculation of complex equilibrium compositions and applications, Tech. Rep. 1311, NASA (1996).

[8] V. P. Zhukov, Computational fluid dynamics simulations of a GO_2/GH_2 single element combustor, J. Propul. Power 31 (6) (2015) 1707–1714.

[9] V. P. Zhukov, M. Pätz, On thermal conductivity of gas mixtures containing hydrogen, Heat Mass Transfer 53 (6) (2017) 2219–2222.

[10] G. Ribert, N. Zong, V. Yang, L. Pons, N. Darabiha, S. Candel, Counterflow diffusion flames of general fluids: Oxygen/hydrogen mixtures, Combust. Flame 154 (3) (2008) 319 – 330.

[11] C. J. Roy, Grid convergence error analysis for mixed-order numerical schemes, AIAA J. 41 (4) (2003) 595–604.